



TECHNICAL ARTICLE

Effect of Cr Addition on the Milling Process and Properties of Nanostructured Cu Alloys Prepared by Mechanical Alloying

Litao Han , Jianwei Liu, Huaguo Tang, and Zixiang Yan

Submitted: 3 September 2021 / Revised: 20 December 2021 / Accepted: 5 April 2022 / Published online: 13 May 2022

Although nanostructure offers several advantages in improving the performance for Cu alloys prepared by mechanical alloying, the excellent properties have not been obtained to date primarily due to a single strengthening method or the Fe contamination introduced by the stainless steel grinding tank and balls. Herein, we added Cr to regulate the milling process and control the content of Fe doped into the Cu matrix. And the effects of Cr on the morphology, crystallite size, lattice strain and properties of Cu were studied. The results showed that adding an appropriate amount of Cr could prevent more Fe from being doped into the alloy matrix. When the Cr content was lower than 0.2 wt.%, the work hardening could be accelerated, so that the Cu alloys had smaller crystallite size, greater internal strain and higher tensile strength. But with continuous increase in Cr content, the crystallite sizes of the alloys began to increase again. Nevertheless, the nanostructured Cu alloys with particle size less than 10 nm were still obtained. In conclusion, by appropriately adjusting the Cr content, we demonstrated an improvement in the properties of the Cu alloys. The optimum properties were achieved by Cu-0.2 wt.% Cr with tensile strength of 517 MPa, ductility of 7.28% and electrical conductivity of 73.37% IACS. And the study provided a new idea for overcoming the Fe contamination in the metal matrix, and further improving high-performance Cu alloys through the combination of fine-grain strengthening and alloy strengthening.

Keywords ball milling, chemical analysis, electrical conductivity, high-performance Cu alloys, mechanical alloying, mechanical testing

1. Introduction

Due to its excellent electrical properties, copper (Cu) is widely used in many fields such as aerospace, nuclear energy and electronics. However, the low strength of Cu limits its further application (Ref 1, 2). To increase the mechanical strength of Cu, plenty of enhancement methods are used such as solid solution (Ref 3, 4), fine particles (Ref 5), dispersion (Ref 6-8) and phase transforming strengthening methods (Ref 9). It is well known that the properties of materials mainly depend on their microstructures. So fine crystal reinforcing has attracted more attention than other methods due to the fact that

nanomaterials have more advantages than coarse-grained materials in improving the performance. This is because the grain boundary's surface-to-volume increases with the decrease in grain size, resulting in a good deal of atoms located in the interface region (Ref 10). For coarse-grained materials, this percentage can be basically ignored, and it is this noticeable disparity that is primarily responsible for the major difference and often superior performance of nanomaterials (Ref 11). Numerous studies have shown that the mechanical properties of pure Cu with nanocrystalline structure are significantly improved, while the electrical conductivity is only slightly decreased (Ref 12-18). In addition, nanocomposites also have many advantages in improving the strength of Cu. The nanoscale second phase or precipitation in the Cu matrix is the obstacle to dislocation movement which increases the strength. Similarly, the conductivity of Cu composites will also decrease. The main reasons are effects of crystallographic defects and the precipitation in electron movements (Ref 16-18).

A lot of methods have been used to produce nanostructured alloys or metal matrix composites reinforced by nanoparticles including powder metallurgy (Ref 19), severe plastic deformation (SPD) (Ref 20, 21), laser melting (Ref 22), and high-energy ball milling (Ref 23). Among these ways, mechanical alloying (MA), due to the simple eco-friendly process and homogenous dispersion of the second phase, has a special place for the production of Cu composites. MA is a powder treatment technology that includes repeated welding, fracturing, and rewelding of powders in milling equipment (Ref 24, 25). And as a non-equilibrium process, MA is considered to be an effective method for preparing nanometer materials because of

Litao Han, Key Laboratory for Special Functional Materials of MOE, National and Local Joint Engineering Research Centre for High-efficiency Display and Lighting Technology, School of Materials, Collaborative Innovation Centre of Nano Functional Materials and Applications, Henan University, Kaifeng 475004, China; and State Key Laboratory of Rare Earth Resources Utilization, Changchun Institute of Applied Chemistry, No. 5625 Renmin Street, Changchun Jilin 130022, China; and **Jianwei Liu**, **Huaguo Tang**, and **Zixiang Yan**, State Key Laboratory of Rare Earth Resources Utilization, Changchun Institute of Applied Chemistry, No. 5625 Renmin Street, Changchun Jilin 130022, China. Contact e-mail: hlt@henu.edu.cn.

the significant deformation introduced into the powders (Ref 17, 26-32). However, since the milling balls and jar are mainly composed of stainless steel, the Cu powders are easily contaminated with iron (Fe) during the milling process. Azimi reports that the content of Fe is about 0.2 wt.% in Cu-Zr alloys milled for above 90 h, which has a small or even negligible impact on the performance of the alloy (Ref 33). However, the research of Viet shows that there is still about 0.8 wt.% Fe in the Cu alloy powders, although the contamination from milling tools has been reduced by controlling the milling rotation (Ref 34). Zhuang et al. even note that more Fe will be detected when the horizontal miller is used to produce Cu matrix composite (Ref 35). Herein, there is more Fe doped into the milled powders because of the difference in high-energy milling equipment and conditions. And the excess Fe is more likely to exist in the form of dispersed state in the Cu matrix because the maximum solubility of Fe in Cu is even less than 0.1 wt.% at 600 °C. Although the excess Fe can increase the nanostructured copper's tensile strength (Ref 36, 37), it will also result in a significant reduction in conductivity, namely 9.2 $\mu\Omega$ cm/wt.% Fe (Ref 38). Therefore, the content of Fe doped into the Cu powders should be controlled.

Many methods have been used to reduce or avoid the introduction of Fe, such as optimizing milling parameters (including milling time (Ref 39), milling rotation (Ref 34)), using appropriate process control agent (PCA) (Ref 40), and selecting milling tanks with the same composition as the raw materials (Ref 33, 41). However, these processes usually lead to the reduction of milling efficiency, which increases the consumption of energy and capital. Adding alloying elements may be a simple and effective method to reduce the Fe content in Cu. Some research results show that Fe and phosphorus (P) can react to form precipitates (Fe_3P or Fe_2P , for instance) during aging, which reduces the Fe content in the Cu (Ref 42-45). Our previous study has also found that the addition of P during MA can effectively reduce Fe content doped from the milling equipment and improve Cu alloys' performance by affecting the ball milling efficiency (Ref 46). However, P has lower ignition point and higher activity. It is particularly prone to spontaneous combustion in air. This causes great risks during the MA process. As a metallic material with BCC lattice system, chromium (Cr) has higher hardness and lower elongation than Cu with an FCC lattice system (Ref 47). Therefore, it may be used to reduce the Fe content doped into the Cu matrix by affecting the milling process of Cu powders during MA (Ref 4). Besides, Cr can optimize the mechanical properties of pure Cu and has more minor damage to electrical conductivity than Fe and P (Ref 48, 49). Fernee has reported that when the Cr content in the Cu matrix is supersaturated, a high degree of thermodynamic metastability will be formed, resulting in a high chemical potential for Cr precipitation. The excellent tensile strength of Cu alloy comes from these nanosized Cr-rich precipitates dispersed in the Cu matrix. At the same time, because of the low concentration of Cr in Cu solid solution (Ref 50-52), the conductivity of Cu alloy is almost indistinguishable from that of pure Cu. However, excessive Cr can also damage the conductivity of the Cu. So the amount of Cr must be kept within a small range.

On the other hand, the high chemical affinity of Cr to Fe may promote the coprecipitation of Fe and Cr in the form of separated phase, solid solutions or Fe/Cr intermetallic compounds. In this case, the net precipitation potential would be much more enormous than that of the binary Cu-Fe, and higher

conductivity would be anticipated (Ref 53). Therefore, although there have been many studies on the effect of Cr content on the morphology, crystallite size and properties of Cu alloys prepared by MA (Ref 10, 17, 29, 51, 54), little attention has been paid to its impact on Fe contamination in milling process. The detailed effects of Cr on the Fe content and the phase of the precipitates formed in the Cu matrix are also not clear. The influence of these factors on the properties of Cu also needs to be studied.

2. Materials and Methods

2.1 Preparation of the Alloys

The Cu powders with the purity of 99.9% and particle size of less than 48 μm and Cr powders with 99.9% purity and particle size of less than 10 μm were selected as starting materials. The purity and particle sizes of the precursors were obtained from the supplier. Then the powders with different proportions were mixed and milled in a stainless steel pot under the protection of argon for 4 h at room temperature using a GN-2 high-energy milling equipment (Shenyang Suntech Instruments Co., Ltd., China). The total weight of the mixed powders was 40 grams. The samples with Cr content of 0, 0.1, 0.2, 0.3, 0.4 and 0.5 wt.% were named S0, S1, S2, S3, S4 and S5, respectively. The weight of the steel balls was 150 grams. So the ball-to-powder weight ratio was 15:4. The ball grinding speed was 532 rpm. An organic solvent of acetone was used as a process control agent (PCA) to avoid over agglomeration of the powders.

Then the milled powder particles were cold-pressed in a closed rectangular mold using a hydraulic press with a pressure of 510 MPa at room temperature. The dwell time was 1 min. The size of the green compact was 60 \times 8 \times 10 mm (length \times width \times height). The model of the tablet press was 769YP-150F produced by Tianjin Keqi High & New Technology Corporation.

The green compacts were then sintered in a modified hot-pressing (HP) furnace according to the following steps.

- (a) Heat the furnace to the required temperature (600-700 °C) with the stainless steel die inside. The heating rate is set to 5 °C min^{-1} .
- (b) Keep the mold warm for 15 min.
- (c) Put the sample into the furnace rapidly, and raise the pressure to 350 MPa on the die in three minutes.
- (d) Take out the sintered specimen and grind the sample surface flat after cooling it to room temperature.

2.2 Characterization

The morphologies of the milled powders with different Cr addition were observed by a Hitachi S-4800 scanning electron microscopy (SEM) under an accelerating voltage of 10 kV. The elemental components of milled powders were analyzed quantitatively by inductively coupled plasma (ICP) (ThermoScientific iCAP6300). The detection limit of typical elements could reach ppb level, and the error percentage of device was less than 2%. The compositions, crystallite sizes and lattice strain of the Cu alloys were identified by x-ray diffraction (XRD, Bruker D8 FOCUS) with a scanning rate of 4° per min

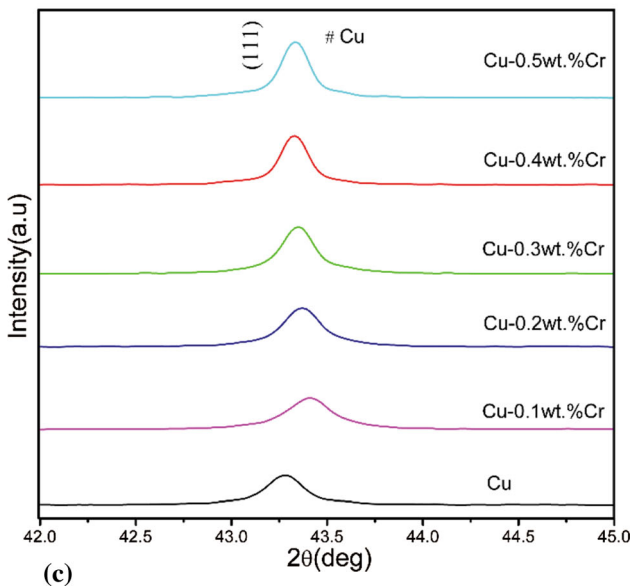
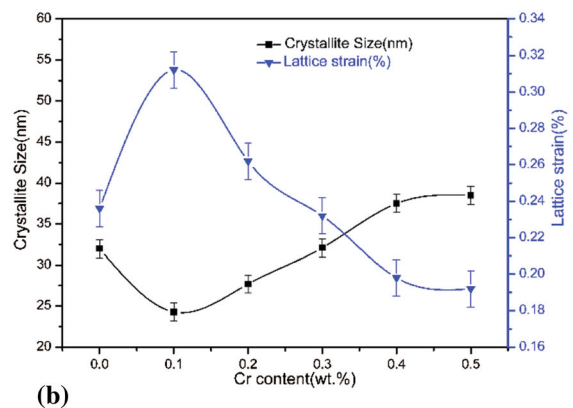
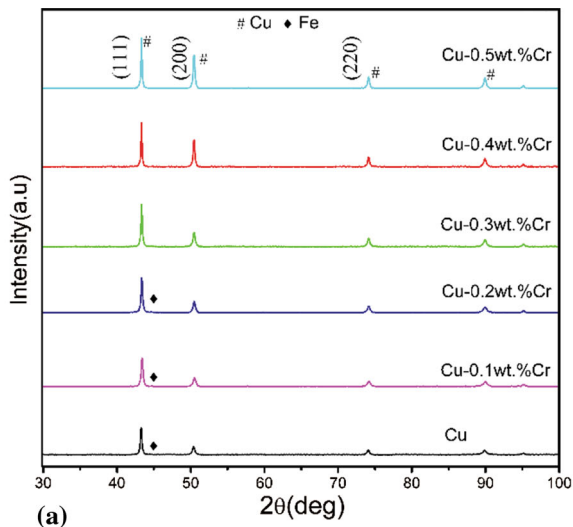


Fig. 1 (a) XRD results of the milled powders varying with Cr content, (b) the variation of average crystallite size and lattice strain of the milled powders varying with Cr content and (c) the partially enlarged view of (a)

operating at 40 mA and 40 kV. In order to ensure the accuracy of the results, the diffraction data were refined by Rietveld. Considering the broadening effect on diffraction peaks caused

Table 1 The main components of the sintered alloys measured by inductive coupled plasma (ICP)

Sample	Cr	Fe	C, Zr, Si...	Cu
	wt.%	wt.%	wt.%	wt.%
S0	0	2.187	$< 1.000 \times 10^{-3}$	Balance
S1	0.0954	2.279	$< 1.000 \times 10^{-3}$	Balance
S2	0.2033	2.058	$< 1.000 \times 10^{-3}$	Balance
S3	0.3101	1.924	$< 1.000 \times 10^{-3}$	Balance
S4	0.3987	0.5743	$< 1.000 \times 10^{-3}$	Balance
S5	0.5221	0.2884	$< 1.000 \times 10^{-3}$	Balance

by micro-strain and reduction in crystallite size, the Stokes and Williamson–Hall formula was used to calculate the Cu crystallographic parameters including crystal size and internal strain (Ref 55). This method could distinguish the effects of two factors on diffraction peak broadening.

$$\beta = \beta_d + \beta\epsilon = K \lambda / (d \cos \theta) + 4\epsilon \tan \theta \quad (\text{Eq 1})$$

where β was the full width at half maximum (FWHM) of the diffraction peak after instrument correction; β_e and β_d were FWHM caused by internal stress and small crystallite, respectively; ϵ and d were internal stress and crystallite size; λ was the wavelength of the x-ray radiation; θ was the Bragg angle; and K was constant as 0.9. The nanostructures of the powders after ultrasonic dispersal in alcohol for 15 mins were also observed by an FEI Tecnai G20 transmission electron microscopy (TEM) operating at 200 kV equipped with energy-dispersive spectroscopy (EDS). The surfaces of the sintered samples firstly were polished by abrasive sandpaper in order with different mesh of 280, 600, 800, 1000, 2000, and 3000. Then they were polished using silica polishing creams (5 nm). After that, the microstructures of the sintered alloys were investigated by SEM. Similarly, the nanostructure of the sintered alloy was proved using TEM. Of course, the specimens first need to be polished into thin foils with a thickness of 50 μm mechanically followed by ion milling.

The densities of the alloy blocks were tested through Archimedes' immersion method. By dividing the measured density by the theoretical density of pure Cu which was 8.92 g cm^{-3} , the relative density was calculated. And the dog-bone shaped alloys were made on the basis of the ASTM E8/E8M-13a standard. The size was about 65 \times 9 \times 3 mm (length \times width \times height). Then tensile strengths were tested by the Instron 4206 universal testing machine. The stretching speed was 10 mm min^{-1} . And the electrical conductivities were measured by the digital double bridge (QJ36a) using the 4-probe method. The international annealed copper standard (IACS) (100%) was used as the standard calibration.

3. Results and Discussion

3.1 Analysis of Milled Powders

XRD spectrum of the mixed powders milled for 4 h with different Cr content is shown in Fig. 1(a). The diffraction peaks corresponding to Cu were intelligibly seen. And the characteristic peaks of Cr or Cu-Cr metallic compounds were not found due to the low content. When the addition amount of Cr was 0.1 wt.%, the diffraction peak of Cu became broaden and the intensity

decreased. However, the noticeable peak sharpening occurred with the increase in Cr content, which indicated the increase in the crystallite size of Cu. The detailed variations of lattice strain and crystallite size for Cu varying with Cr content are shown in Fig. 1(b). It could be seen that the crystallite size of Cu powders decreased first and then increased with the content of Cr. The detailed crystallite sizes were 32.0 ± 0.9 , 24.3 ± 1.1 , 27.7 ± 1.0 , 32.1 ± 0.8 , 37.3 ± 0.9 , 38.5 ± 1.2 nm, respectively. Generally, the crystallite size was determined by the competition between plastic deformation through the motion of dislocations, and the recovery and recrystallization (Ref 56). Crystallite sizes were related to the generations and pile-ups of

dislocations caused by the plastic deformation. Severe plastic deformation led to the increase in dislocation densities which would form cell walls and cell structure. And under higher cold working conditions, these cell structures might transform into crystal boundaries (Ref 4, 24, 51). When the Cr content was below 0.2 wt.%, adding Cr particles into the Cu powders could increase work hardening through producing dislocation forests and intense dislocation pile-ups. Therefore, the crystallite size of the milled powders decreased. This was also consistent with the increase in lattice strain caused by the stress field, which was created by the dislocation multiplication because of the severe plastic deformation introduced into the powder particles (Ref 57).

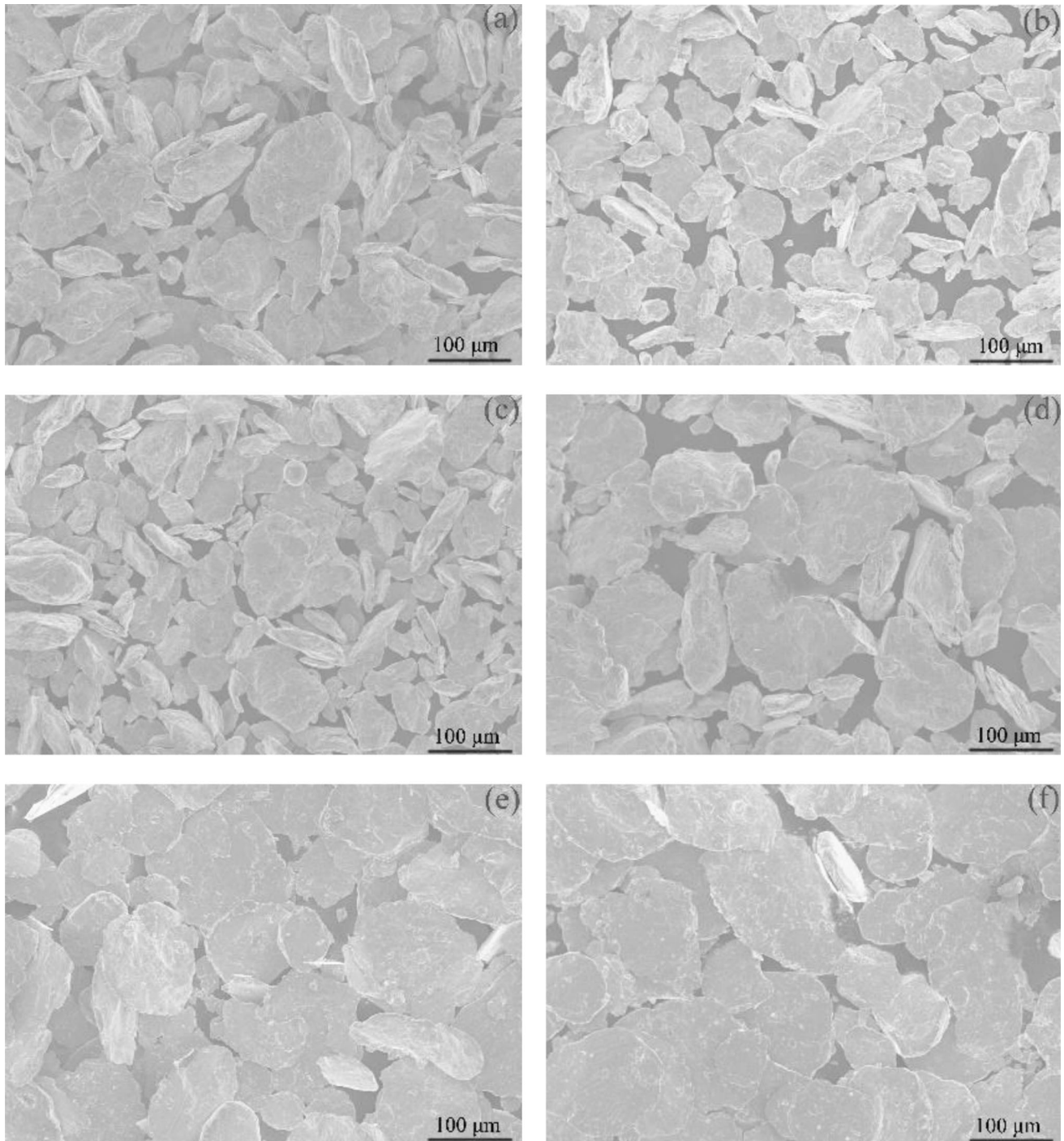


Fig. 2 SEM of the powders milled for 4 h with (a) 0 wt.%, (b) 0.1 wt.%, (c) 0.2 wt.%, (d) 0.3 wt.%, (e) 0.4 wt.% and (f) 0.5 wt.% Cr

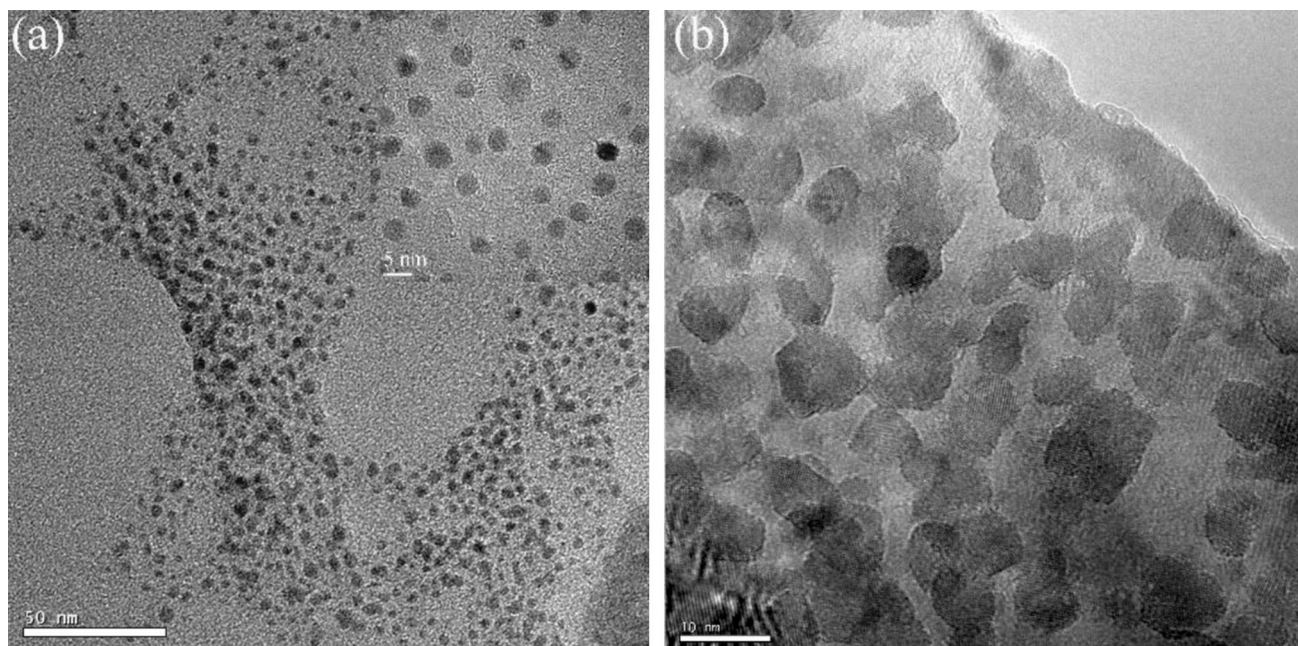


Fig. 3 TEM images of (a) the powders with 0.1 wt.% Cr and (b) the sintered samples with 0.1 wt.% Cr

Moreover, many studies had shown that higher initial proportion of alloying elements could accelerate work hardening. That was to say, by increasing the percentage of the Cr, the effects of the cold working should become more apparent, and as a result, the crystallite sizes should be smaller (Ref 10, 54, 58). However, in this study, it was evident that crystallite size began to increase gradually, whereas lattice strain decreased with the continuous increase of Cr content. This might be because the work hardening effect was weakened by excessive Cr for some reason. At the same time, in the milling process, violent impacts of stainless steel balls on Cu particles led to the increase in mechanical contact between particles. Then the temperature of the particle surfaces could rise locally due to energy transfer (Ref 24). If the temperature rose sharply, the crystal would undergo recovery and recrystallization processes, which led to a decrease in dislocation density and an increase in crystallite sizes (Ref 56, 59).

Figure 1(c) is the partially enlarged view of Fig. 1(a). It could be seen that there was a slight drift of the characteristic peaks of Cu toward a higher diffraction angle compared with milled Cu without Cr addition. It suggested that solid solution formation occurred when the strain reached an extremely high value and crystallite size became relatively small. And the peak shifts were caused by the solid solution of Cr into the Cu matrix, which was also consistent with the fact that the atomic size of Cu was larger than that of Cr (Ref 60, 61). There were different views on the formation mechanism of solid solution by MA (Ref 62-65). During the milling process, the decrease in crystallite size increased the grain boundary area, which provided more diffusion paths for Cr to diffuse into the Cu lattice. In addition, due to the increase in internal energy caused by a large number of defects, the activation energy required for Cr diffusion was decreased (Ref 62, 63). Veltletal's research showed the stored energy of the grain boundary volume of nanomaterials was the main driving force of the solid solution formation. Therefore, solute atoms tend to substitute solvent atoms on grain boundaries. Yavarietal (Ref 65) reported that severe plastic deformation was one of the main reasons to

promote the formation of solid solution. The capillary force generated by the small microcrystals (less than 2 nm) formed at the tip of broken powder particles promoted the diffusion of solute atoms and improved the solid solubility. Taghian also reported that the high temperature caused by cold working could facilitate the solution of Cr into Cu crystals. The results in this paper also showed that nanocrystallite size and severe plastic deformation were the main reasons for the formation of Cu-Cr solid solution. Generally speaking, more Cr content in the original mixture could result in a higher concentration gradient of Cr atoms in the Cu matrix and then more Cr atoms diffused into the Cu crystal. However, in this paper, the shift of Cu diffraction peak to higher angle was slightly weakened with the increase in Cr content in the initial powder mixture, which indicated that the solute Cr content decreased gradually. This was related to the decrease in lattice strain and increase in crystallite size mentioned above.

Moreover, the diffraction peak of Fe could be seen when the Cu powders were milled for 4 h without Cr addition. Fe particles entered the powders through the collision between steel balls and the grinding pot. To determine the Fe contents in the Cu powders, inductively coupled plasma (ICP) was performed, as shown in Table 1. The results showed that as Cr content increased from 0 to 0.5 wt.%, the Fe contents were 2.187, 2.279, 2.058, 1.924, 0.5743 and 0.2884 wt.%, respectively. When the Cr content added was about 0.1 wt.%, the Fe content doped in the powder increased. This was because the presence of Cr in the Cu matrix could increase the rate of work hardening and promote the fracture of Cu particles. During milling, Cr particles (BCC crystal system) which were more brittle than ductile Cu particles (FCC) fractured firstly. The broken fine Cr particles were then randomly distributed among the cold-worked Cu particles, which promoted the crack propagation into Cu particles and made the Cu fracture. Therefore, the finer particles provided more surfaces and paths for more Fe atoms to diffuse into Cu. In addition, due to the local high temperature on the particle surface, Fe atoms could

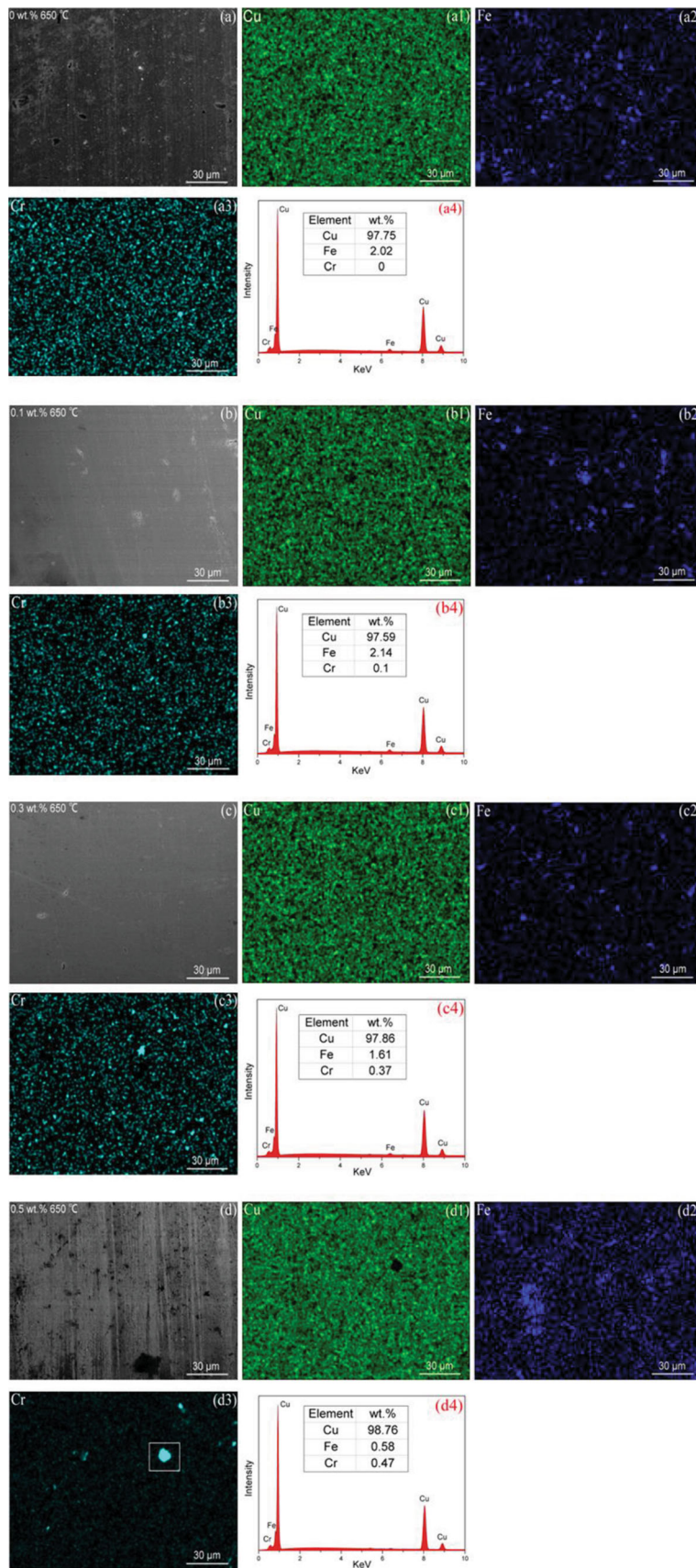


Fig. 4 The mapping of elements distribution and the corresponding EDS spectra data of Cu alloys sintered at 600 °C with (a) 0 wt.%, (b) 0.1 wt.%, (c) 0.3 wt.% and (d) 0.5 wt.% Cr

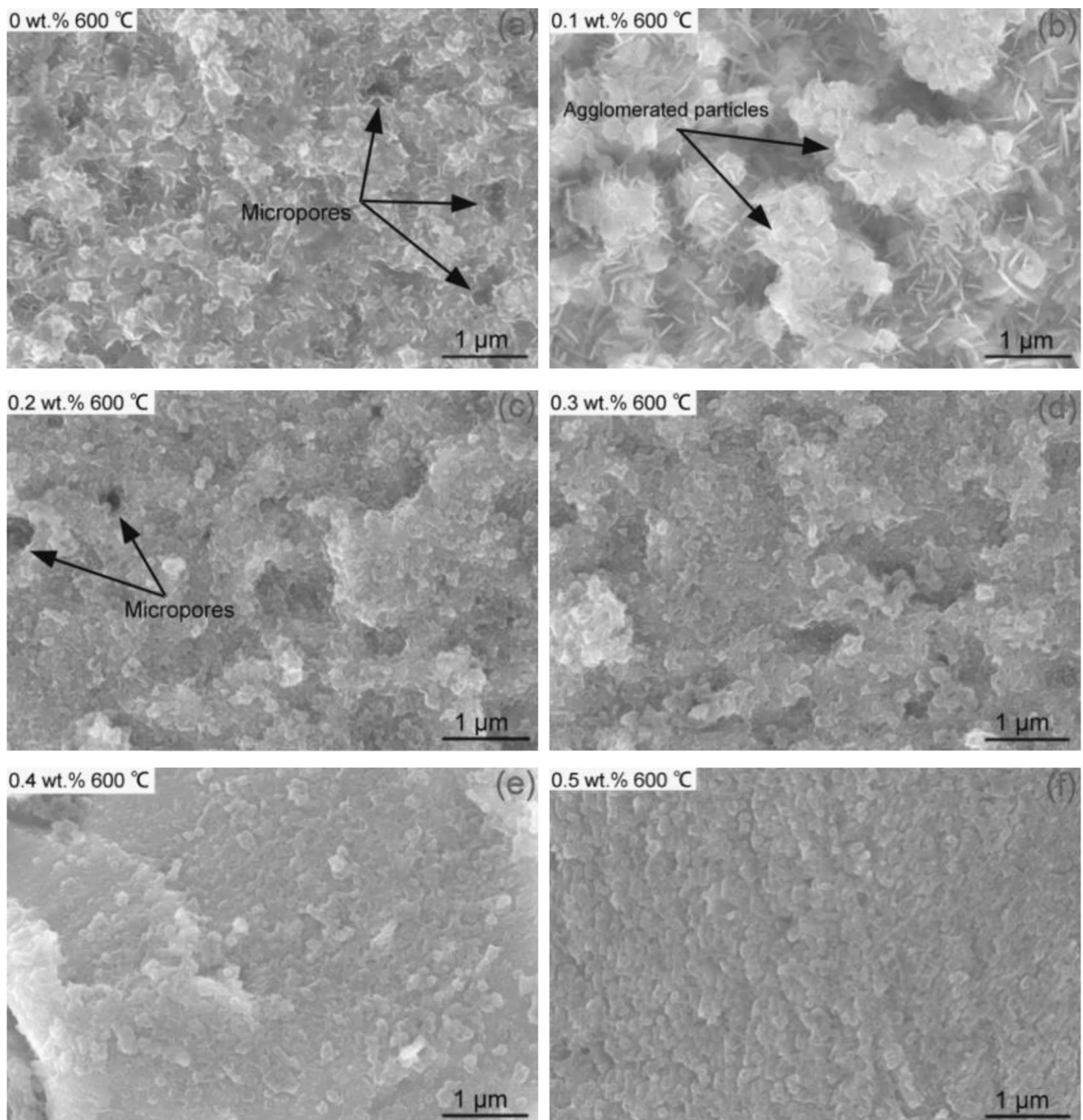


Fig. 5 SEM images of the Cu alloys with different Cr content sintered at 600 °C

diffuse into the Cu matrix in the milling process. And considering the atomic radius of Fe (0.126 nm) and Cu (0.128 nm), Fe dissolved in Cu matrix should form a substitutional solid solution, which would not cause obvious shrinkage of the Cu lattice. However, when the added Cr content exceeded 0.2 wt.%, the Fe content in the powders began to decrease. It was also due to the fact that adding more Cr could affect the milling process. The role of the added Cr was similar to that of PCA, which mitigated the sharp increase in collision energy during MA. Therefore, the grain refinement degree and Fe content were both correspondingly reduced. It could also be demonstrated by SEM images of the powder mixtures with different Cr content after milling for 4 h. The

average particle size of the powder mixture without Cr addition was about 60 μm appearing as an irregular ellipse or strip shown in Fig. 2(a). When the added Cr content was less than 0.2 wt.%, they could increase the work hardening rate and promote the fracture of Cu particles. Therefore, the particles became finer and more evenly distributed. Similarly, with the continuous increase in Cr content, the powder particles gradually became flaky with larger size. This was consistent with the changing trend of crystallite sizes and Fe content discussed above.

Thereafter, the nanostructures of the mixed powders were characterized by TEM. The microstructure of the alloy powders containing 0.1 wt.% Cr is shown in Fig. 3(a). It could be seen

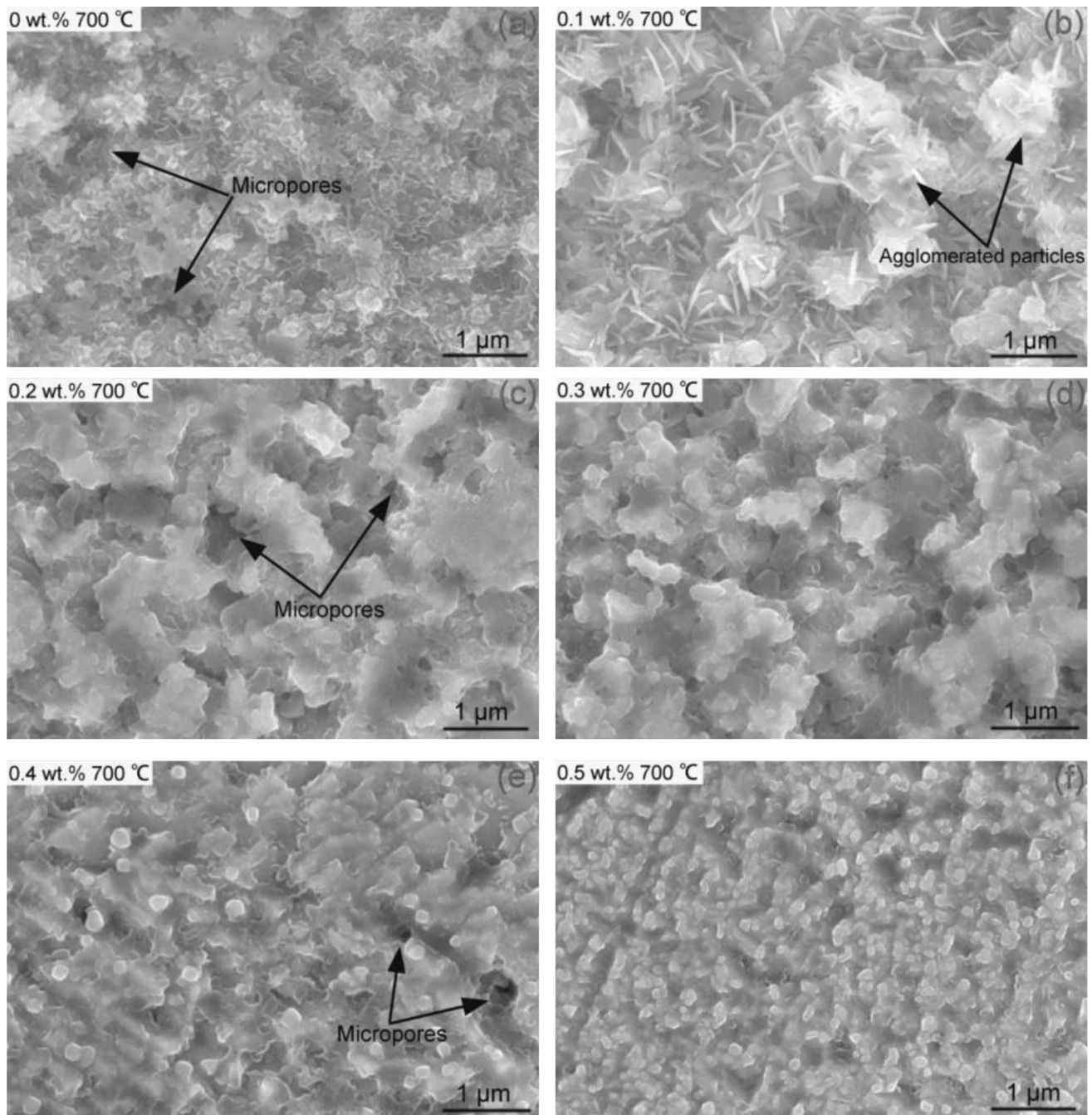


Fig. 6 SEM images of the Cu alloys with different Cr content sintered at 700 °C

that the powders presented irregular nanoscale spheres with a particle size of nearly 5 nm.

3.2 Analysis of Sintered Samples

In order to analyze the microstructures and properties of the sintered samples, the powders were firstly sintered into blocks through hot-pressing. Then, TEM was carried out to further confirm the nanostructure of the alloys. Figure 3(b) shows the TEM images of the sintered sample milled for 4 h with 0.1 wt.% Cr. It is revealed that the particles of the alloy sample showed an irregular circular pattern with a uniform size of nearly 10 nm. This proved that the sintering method was an effective way to prepare nanoblocks.

However, the distributions of Fe and Cr in the alloys were still unclear. The way in which Fe and Cr existed in the sintered samples and whether intermetallic compounds of Cu_xCr_y formed were still the key issues affecting the properties of the materials. Therefore, the composition distributions of the Cu alloys were confirmed by recording SEM/EDS elemental mapping (Fig. 4a-d). It was observed that the excess Fe doped during the milling process was distributed randomly in the Cu matrix and accumulated in different degrees when the Cr content was less than 0.3 wt.%. Based on the binary phase diagram of Cu-Fe alloy, the solid solubility of Fe in Cu was very low, which was still less than 0.1% at 600 °C. And there was neither reaction nor dissolution between the two compo-

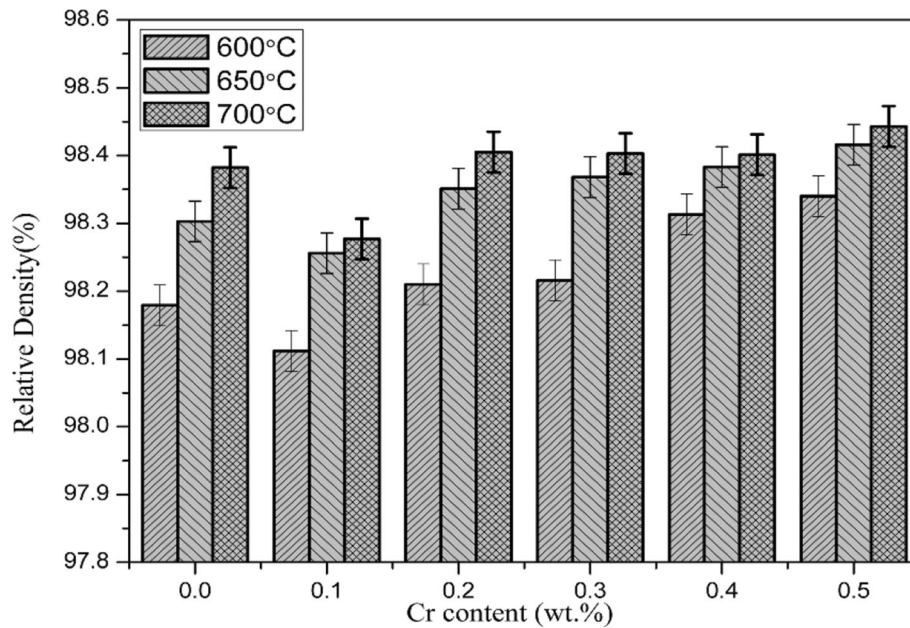


Fig. 7 Densities of the sintered samples plotted versus Cr content and sintering temperature

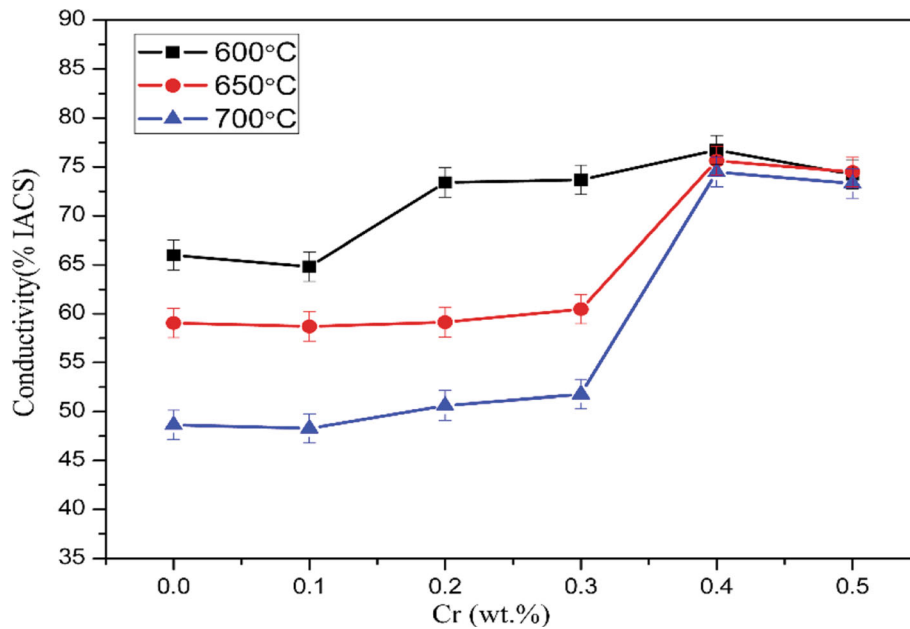


Fig. 8 Electrical conductivities of the Cu alloys varying with Cr content and sintering temperature

nents of Cu and Fe. As a non-equilibrium process, MA could be used to improve the solid solubility between Fe-Cu (Ref 66-68). The maximum solubility of Fe in Cu was 4.1 wt.%, and in the literature it was reported that the maximum practical limit is ~ 2.5 wt.% (Ref 53). In this paper, the high milling speed (532 rpm) and time (4 h) also increased the solubility of Fe in Cu. However, due to the low sintering temperature and high Fe content, it was difficult for these Fe to be completely dissolved in Cu matrix. Therefore, the excess Fe would exist in the Cu matrix in the elemental state. These enriched Fe would also seriously affect the densities and conductivities of the alloys. Fortunately, the aggregation of Fe was weakened with the

continuous addition of Cr. And the distribution of Fe became more uniform as Cr content increased to 0.5 wt.%, which can be seen in Fig. 4(d2). The EDS results also showed that when the content of Cr increased to 0.5 from 0.1 wt.%, the content of Fe decreased to 0.58 from 2.14 wt.%. Besides, the values of Fe measured by EDS were slightly higher than the ICP results. This was because the analysis object of ICP was larger than the EDS, which only counted the local area of the alloy. This further indicated that the distribution of Fe in the alloy matrix was not completely even. In addition, when the Cr content was relatively low, it was uniformly dissolved in the Cu matrix. However, when the Cr content exceeded 0.3 wt.%, it also

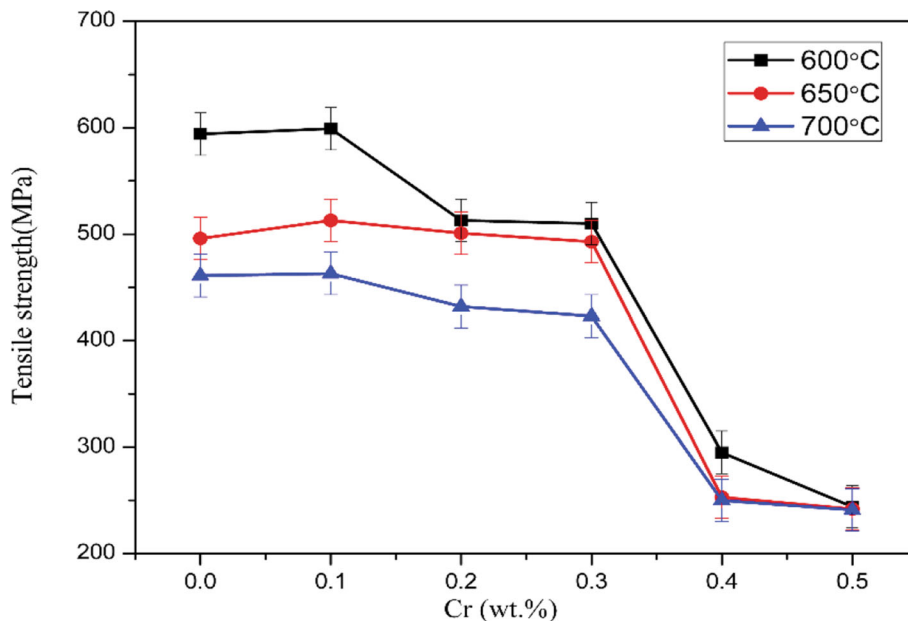


Fig. 9 Tensile strengths of the Cu alloys varying with Cr content and sintering temperature

began to accumulate in the Cu matrix, which is presented in Fig. 4(c3) and (d3). This could also cause severe damages to the electrical conductivities of the alloys. So the Cr content must be controlled less than 0.3 wt.%. H. Fernee also showed that the addition of more Cr than 0.7 wt.% would serve no purpose in the precipitation hardening of the alloy and might have damage to the electrical conductivity (Ref 53). Besides, Fe and Cr were not concentrated together. Although Fe and Cr had a high chemical affinity and completed solid solubility in one another at elevated temperatures, they had not reacted with each other to form intermetallic compounds. This may be because the composition would have the highest thermodynamic driving force for the precipitation reaction into the FeCr σ phase only when the ratio of Fe to Cr was 0.7-0.8 wt.% (Ref 53).

The microstructures of sintered alloys would be different due to the changes of crystallite sizes and morphologies of the milled powders with varying Cr content. And this was a big deal in terms of alloys' performance. Therefore, the surface morphologies of the Cu alloys sintered at 600 and 700 °C were tested by SEM as illustrated in Fig. 5 and 6, respectively. It could be seen that the sintered block without Cr addition was composed of many particles with different shapes such as strips or flakes. These particles were formed by the agglomeration of nanoparticles with high surface energy. And due to the different shapes and sizes of these particles, many micropores existed in the alloy during sintering. When the content of Cr was added to 0.1 wt.%, the powder particles became rigid after serious cold working, making it more difficult for the powders to fully contact with each other during low-temperature sintering. Therefore, the particles aggregated together, and a lot of voids were formed. The compactness of the alloy became slightly worse. However, as Cr content continued to increase, the cold working of the powder particles induced by Cr addition was weakened. This allowed the particles to bind more tightly together to improve the compactness of the alloy. Moreover, Cr was more reactive than Cu. So the excess Cr was more likely to combine with the oxide layers on the surface of Cu powders

generated during storage when the powders were sintered. Then the loss of the oxide layers would expose more fresh and active Cu atoms and reduced their diffusion activation energy, which accelerated the bonding process between Cu particles.

It also could be seen that there were fewer pores in the alloys sintered at 700 °C. The structures were more compact than those sintered at 600 °C. The powder particles sintered at 600 °C were densified by metallurgical bonding with each other, which was mainly a solid-state sintering process. Due to the lack of liquid phase migration in the sintering process, it was difficult for the particles to contact completely. Therefore, in addition to the obvious micropores between agglomerated particles, there were more gaps between finer particles. When the sintering temperature rose to 700 °C, some liquid phase appeared in the samples during the sintering process. The solid particles were displaced and adjusted under the action of liquid surface tension, so as to achieve the closest arrangement. Then more micropores and smaller gaps in the alloy were effectively filled. Furthermore, the increase in sintering temperature was more favorable to the diffusional mass transfer process through a variety of pathways, such as lattice, grain boundaries and defects/dislocations (Ref 57). And high temperature could offer more energy for the atoms to bond together and make it easier for the gas to escape from the alloy.

Sintering densification was a prerequisite for alloys to obtain excellent properties. Meanwhile, in order to further verify the above conclusions, the change in densities of the prepared Cu alloys is analyzed in Fig. 7. It showed that the density decreased slightly when the content of Cr addition was 0.1 wt.%. However, the densities began to increase gradually as the Cr content continued to increase. This was completely consistent with the structural evolution mentioned above. The compactness of the sintered alloys was also related to the amount of Fe and Cr in the Cu matrix. The sintering process mainly happened between Cu powders. So the Fe and Cr with higher melting points inhibited the bonding of Cu powders during sintering which caused cavities. Coincidentally, the

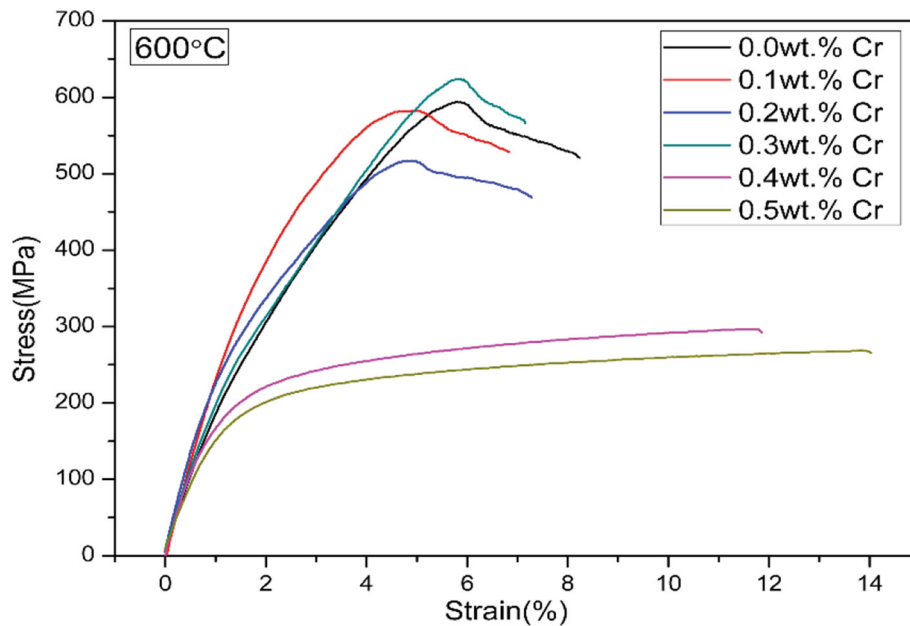


Fig. 10 Stress–strain curves of the Cu alloys sintered at 600 °C

addition of Cr also reduced the Fe content in the alloy, which promoted the bonding of Cu powders. It also could be seen that the densities of the alloys sintered at high temperatures were larger than those sintered at low temperatures.

3.3 Properties

The relationship between sintering temperature and alloys' properties can be seen in Fig. 8 and 9. The alloy samples exhibited low tensile strength and electrical conductivity at higher sintering temperature, which was consistent with our previous results (Ref 46, 69). Sintering at higher temperature resulted in more grain coarsening. The strengthening effect of fine crystal was weakened, and then the tensile strength decreased. And it was also easy for the samples to be oxidized at high temperature. Those oxides deposited in the Cu matrix would increase the electron scattering and then decrease the electrical conductivity.

The electrical conductivities of the alloys are illustrated in Fig. 8. As could be seen from the figure, the electrical conductivity was reduced when the Cr addition was 0.1 wt.%. This might be owing to the decrease in crystallite size, solid solution of Cr and increase in Fe content. When the Cr content added was below 0.1 wt.%, it was almost equivalent to the Fe content reduced in the alloy. The reduction of Fe content on the electrical conductivity of Cu could be estimated through the following theorem:

$$\delta = \delta_0 \left[1 - \frac{f}{(1-f)/3 + \delta_0/(\delta_0 - \delta_1)} \right] \quad (\text{Eq 2})$$

where δ was the conductivity of the alloy; δ_0 was the conductivity of pure Cu; δ_1 was the conductivity of Fe; and f was the volume fraction of Fe in the alloy. Among them, δ_0 was much greater than δ_1 because the conductivity of Cu was significantly better than that of Fe. Therefore, when the change in Fe content (Δf) was about 0.1 wt.%, δ was approximately equal to $0.999 \delta_0$. This indicated that when the Cr addition was 0.1 wt.%, the conductivity change of the Cu matrix was only

$0.001 \delta_0$, which can be almost ignored. Therefore, the variation of conductivity was mainly influenced by the solid solution of Cr. Due to the difference in atomic sizes, Cr dissolved in Cu could distort the lattice of the Cu matrix. When electrons travelled near the lattice distortion, scattering would occur, which inevitably seriously deteriorated the conductivity of Cu. The conductivity loss of Cu caused by Cr solid solution could be calculated through the Mathiesen theorem (Ref 54),

$$\rho = \rho_0 + \Delta\rho C + K \quad (\text{Eq 3})$$

where C was the solute concentration of Cr; $\Delta\rho$ was the change in resistivity. Hence the change of conductivity caused by Cr solution could be calculated by $\Delta\rho C$. However, with the continuous addition of Cr content, the Fe content in the Cu matrix decreased significantly. Therefore, when the amount of Fe reduced was greater than the amount of Cr added, the conductivity began to increase. Another reason for the higher electrical conductivity was the increase in crystallite size caused by the continued addition of Cr. The increase in crystallite size would result in the decrease of total grain boundary areas. When the electron crossed the grain boundary, the scattering effect on the electron was also weakened.

The tensile strength of the Cu alloy is displayed in Fig. 9. The variation trend of tensile strength was roughly opposite to that of electrical conductivity. When the Cr content added was 0.1 wt.%, the main strengthening effects of the Cu matrix were refined crystalline strengthening and solution strengthening of Cr and Fe. And with the increase in Cr content, the tensile strength began to decrease, which was related to the significant decrease in Fe content and increase in crystallite size.

The corresponding stress–strain curves of the samples sintered at 600 °C are presented in Fig. 10. The elongation of the alloy was 8.2% when Cr was not added into the alloy. When the amount of Cr was increased to 0.1 wt.%, the elongation of the alloy decreased to 6.8%. But with the continuous increase in Cr content, the elongations of the alloys then began to increase. And it reached 14% when the Cr content was 0.5 wt.%. This changing trend was contrary to the variation of

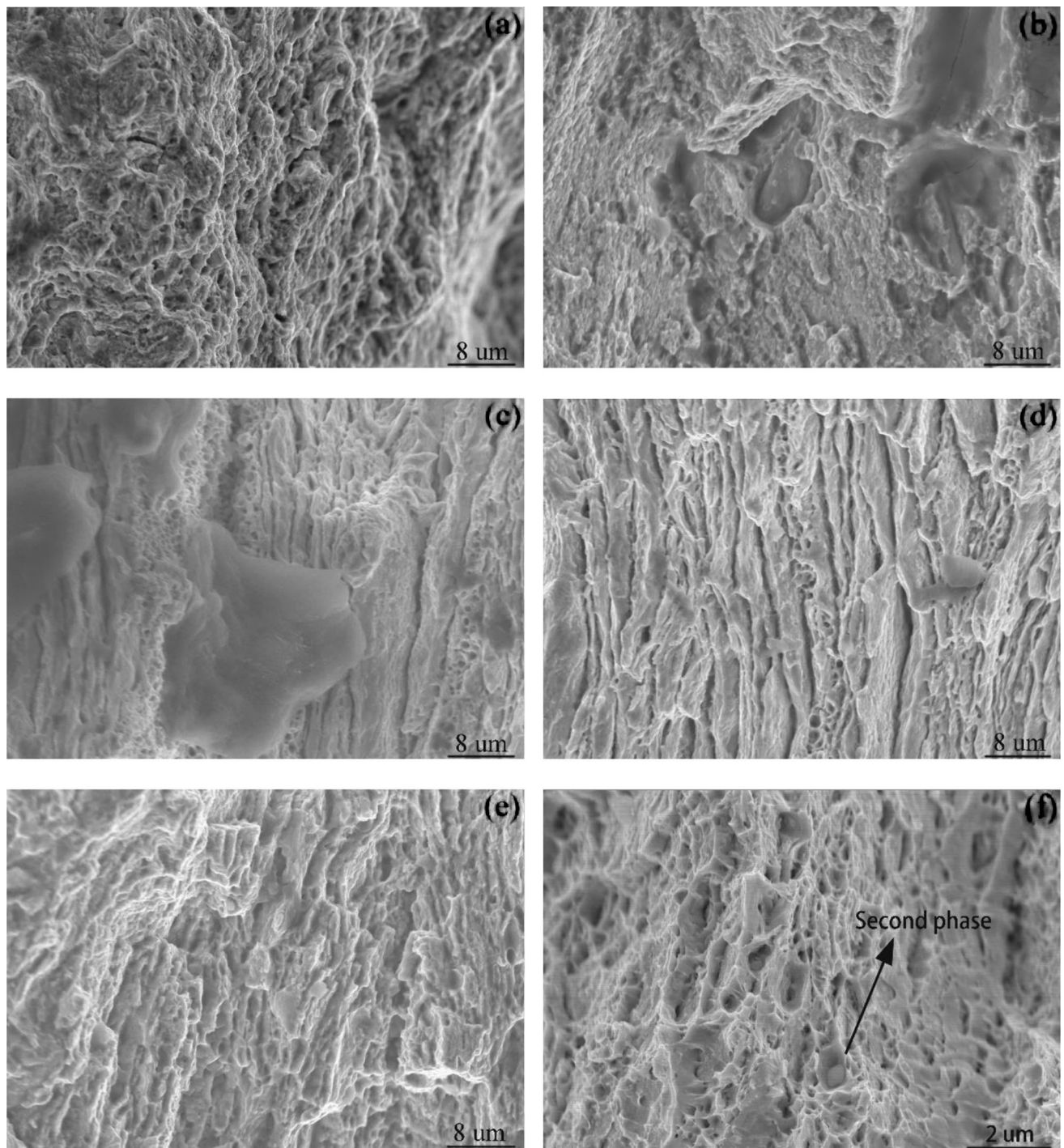


Fig. 11 The fracture morphologies of the tension test samples with (a) 0 wt.%, (b) 0.1 wt.%, (c) 0.2 wt.%, (d) 0.3 wt.%, (e) 0.4 wt.% and (f) 0.5 wt.% Cr

alloys' tensile strengths. Generally, the increase in elongation was related to the formation of dimples. The fracture morphologies of the tension test samples with different Cr content are displayed in Fig. 11. As seen in the figure, the material displayed the fracture features of the dimple fracture. Many dimples of different shape, size and depth were observed in the alloy fracture morphologies. When the Cr content was 0.1 wt.%, the dimple appeared to become shallower and smaller, corresponding to a reduction in plasticity. But with

the addition of more Cr, many obvious slip bands appeared in the fracture of the alloys, and the number of dimples increased gradually. This may be related to the sharp reduction of Fe content in the alloy. When there were more Fe impurities in the material, the microvoids were easier to form near the second phase and begin to grow, coalesce and fracture finally. Therefore, the material showed poor deformation resistance and plasticity. The larger agglomerated particles of second phase had greater harm to the plasticity of the alloy, as shown in

Fig. 11(b), (c). When the content of Fe was significantly reduced, the number of dimples in the alloy was increased significantly and the plasticity of the alloy was also improved, as shown in Fig. 11(f).

The rapid development of emerging industries puts forward higher requirements for the properties of Cu alloys. Therefore, Cu alloy with high strength and high conductivity has become an urgent advanced material. In this paper, the tensile strength of Cu-0.2 wt.% Cr is 517 MPa and the maximum value of electrical conductivity is 73.37% IACS. Considering that the nano-Cu alloy prepared in this paper has excellent comprehensive properties, it is expected to be used in electrical and electronic applications (lead frames, conductive coils, spot-welding electrodes) (Ref 34, 70), nuclear energy (thermonuclear experimental reactor) (Ref 71), as well as in aerospace such as combustion chamber and rocket nozzle, where the ability to remove heat and retain sufficient strength is of critical importance (Ref 72).

4. Conclusions

In summary, the nanostructured Cu alloys were successfully prepared by MA and HP. The particle size of the alloy blocks was nearly 10 nm (TEM). Meanwhile, research results presented in this study revealed the effect of Cr content on the milling process and properties of Cu alloys sintered at different temperatures. Adding 0.1 wt.% Cr could promote the fracture of the powder particles during milling by introducing more cold working. Therefore, the crystallite size of the powders became smaller and the Fe content doped into the powders increased slightly. But with the continuous increase in Cr content, the collision between powders and balls were weakened. Then the Fe content was indeed reduced with just a minor increase in the crystallite size. In addition, although sintering at the high temperature could improve the alloys' compactness, it also could lead to the coarsening of nanograins and damage the properties. By controlling Cr content and sintering temperature, we fabricated a high-performance Cu alloy with electrical conductivity of 73.37% IACS and tensile strength of 513 MPa through the joint action of fine-grain strengthening, second phase strengthening and solid solution strengthening. Our finds also provided a new idea for overcoming the Fe contamination in the metal matrix, and a combination of multiple strengthening methods may be more critical for the further improvement of high-performance Cu alloys.

Acknowledgments

This work was supported by the Funds for Creative Research Groups of China (Grant No. 21521092) and the National Natural Science Foundation of China (Grant No. 52071311).

Conflict of interest

The authors declare that they have no conflict of interest.

References

1. L. Chai, Z. Zhou, Z. Xiao, J. Tu, Y. Wang, and W. Huang, Evolution of Surface Microstructure of Cu-50Cr Alloy Treated by High Current

- Pulsed Electron Beam, *Sci. China Technol. Sci.*, 2015, **58**(3), p 462–469.
2. J.R. Davis, Copper and Copper Alloys, *Corr. Metal/Environ. React.*, 2001, **3**(2), p 527–602.
3. W. Wang, J. Zhu, N. Qin, Y. Zhang, S. Li, Z. Xiao, Q. Lei, and Z. Li, Effects of Minor Rare Earths on the Microstructure and Properties of Cu-Cr-Zr Alloy, *J. Alloys Compd.*, 2020, **847**, 155762.
4. M.T. Dehaqani and G.H. Akbari, Effect of Milling Parameters and Cr Content on Morphology and Solubility of Nanostructured Cu-Cr Solid Solutions, *Trans. Indian Inst. Met.*, 2014, **67**(3), p 385–391.
5. X. Liu, L. Zhuang, and Y. Zhao, Microstructure and Mechanical Properties of Ultrafine-Grained Copper by Accumulative Roll Bonding and Subsequent Annealing, *Mater. Basel, Switzerland*, 2020, **13**(22), p 5171. (in eng)
6. W. Zeng, J. Xie, D. Zhou, Z. Fu, D. Zhang, and E.J. Lavernia, Bulk Cu-NbC Nanocomposites with High Strength and High Electrical Conductivity, *J. Alloys Compd.*, 2018, **745**, p 55–62.
7. A.S. Prosviryakov, SiC Content Effect on the Properties of Cu-SiC Composites Produced by Mechanical Alloying, *J. Alloys Compd.*, 2015, **632**, p 707–710.
8. J. Li, J. Ni, B. Huang, J. Chen, Z. Xu, S. Liao, C. Wang, and W. Luo, Long-Term Ball Milling and Hot Pressing of in-situ Nanoscale Tungsten Carbides Reinforced Copper Composite and Its Characterization, *Mater. Charact.*, 2019, **152**, p 134–140.
9. L. Peng, H. Xie, G. Huang, Y. Li, X. Yin, X. Feng, X. Mi, and Z. Yang, The Phase Transformation and Its Effects on Properties of a Cu-0.12 wt.% Zr alloy, *Mater. Sci. Eng. A*, 2015, **633**, p 28–34.
10. G.H. Akbari and M. Taghian Dehaqani, Nanostructure Cu-Cr Alloy with High Dissolved Cr Contents Obtained by Mechanical Alloying Process, *Powder Metal.*, 2011, **54**(1), p 19–23.
11. D. Roy, M.A. Atwater, K. Youssef, J.C. Ledford, R.O. Scattergood, and C.C. Koch, Studies on Thermal Stability, Mechanical and Electrical Properties of Nano Crystalline Cu99.5Zr05 Alloy, *J Alloys Compd*, 2013, **558**, p 44–49.
12. J. Schiøtz and K.W. Jacobsen, A Maximum in the Strength of Nanocrystalline Copper, *Science*, 2003, **301**(5638), p 1357–1359.
13. C.J. Shen, Z.W. Zhu, and D. Zhu, A Bulk of Uniform Nanocrystalline Copper with Superior Comprehensive Mechanical Properties Electroformed in an Ultra-low Sulfate Concentration Bath without Additives, *Mater. Sci. Eng. A*, **704**(Supplement C), 238–245 (2017)
14. A. Habibi, M. Ketabchi, and M. Eskandarzadeh, Nano-grained Pure Copper with High-Strength and High-Conductivity Produced by Equal Channel Angular Rolling Process, *J. Mater Process Technol.*, 2011, **211**(6), p 1085–1090.
15. L. Lu, Y. Shen, X. Chen, L. Qian, and K. Lu, Ultrahigh Strength and High Electrical Conductivity in Copper, **304**(5669), 422–426 (2004)
16. R.M. Babaheydari, S.O. Mirabootalebi, and G.H. Akbari, Investigation on Mechanical and Electrical Properties of Cu-Ti Nanocomposite Produced by Mechanical Alloying, *Int. J. Eng.* **33**(9), 1759–1765 (2020) (in en)
17. R. Mirahmadi Babaheydari, S.O. Mirabootalebi, and G.H. Akbari Fakhrebadi, Effect of Alloying Elements on Hardness and Electrical Conductivity of CU Nanocomposites Prepared by Mechanical Alloying, *IJST*, **18**(1), 1–11 (2021)
18. L.N. Rajeshkumar and K.S. Amirthagadeswaran, Variations in the Properties of Copper-Alumina Nanocomposites Synthesized by Mechanical Alloying, *Mater. Technol.*, 2019, **53**(1), p 57–63.
19. P.K. Prajapati and D. Chaira, Fabrication and Characterization of Cu-B4C Metal Matrix Composite by Powder Metallurgy: Effect of B4C on Microstructure, Mechanical Properties and Electrical Conductivity, *Trans. Indian Inst. Metals*, 2019, **72**(3), p 673–684.
20. D.A. Aksenov, R.N. Asfandiyarov, G.I. Raab, E.I. Fakhretdinova, and M.A. Shishkunova, Influence of the Chromium Content in Low-Alloyed Cu-Cr Alloys on the Structural Changes, Phase Trans. Proper. Equal-Channel Ang. Pressing, *Metals*, **11**(11), 14, 1795, (2021) (in English)
21. K. Rodak, Cu-Cr and Cu-Fe Alloys Processed by New Severe Plastic Deformation: Microstructure and Properties, ed., 2017
22. C. Gao, M. Yao, C. Shuai, S. Peng, and Y. Deng, Nano-SiC Reinforced Zn Biocomposites Prepared via Laser Melting: Microstructure, Mechanical Properties and Biodegradability, *J. Mater. Sci. Technol.*, 2019, **35**(11), p 2608–2617.

23. A. Fathy, A. Wagih, and A. Abu-Oqail, Effect of ZrO₂ Content on Properties of Cu-ZrO₂ Nanocomposites Synthesized by Optimized High Energy Ball Milling, *Ceram Int*, **45**, (2018)
24. C. Suryanarayana, Mechanical Alloying and Milling, *Prog. Mater. Sci.*, 2001, **46**(1), p 1–184.
25. D. Maurice and T.H. Courtney, Modeling of Mechanical Alloying: Part II. Development of Computational Modeling Programs, *Metal. Mater. Trans. A*, 1995, **26**(9), p 2431–2435.
26. A. Kumar, K. Jayasankar, M. Debata, and A. Mandal, Mechanical Alloying and Properties of Immiscible Cu-20 wt.% Mo Alloy. *J. Alloys Comp.*, **647**, 1040-1047 (2015)
27. J. Zhou, D. Zhu, L. Tang, X. Jiang, S. Chen, X. Peng, and C. Hu, Microstructure and Properties of Powder Metallurgy Cu-1%Cr-0.65%Zr Alloy Prepared by Hot Pressing, *Vacuum*, **131**, 156-163 (2016)
28. K.R. Ramkumar, S. Sivasankaran, and A.S. Alaboodi, Effect of Alumina Content on Microstructures, Mechanical, Wear and Machining Behavior of Cu-10Zn Nanocomposite Prepared by Mechanical Alloying and Hot-Pressing, *J. Alloy. Compd.*, 2017, **709**, p 129–141.
29. A. Torabi, R.M. Babaheydari, G.H. Akbari, and S.O. Mirabootelebi, Optimizing of Micro-hardness of Nanostructured Cu–Cr Solid Solution Produced by Mechanical Alloying Using ANN and Genetic algorithm, *SN Appl. Sci.*, 2020, **2**(11), p 1919.
30. A. Khajesarvi and G.H. Akbari, Synthesis and Structural Characterization of Nanocrystalline Ni₅₀Al₅₀–xMoxintermetallic Compound Prepared by Mechanical Alloying, *Russian J. Non-Ferrous Metals*, 2017, **58**(4), p 411–417.
31. J. Arasteh and G.H. Akbari, Microstructural Evolution During High-energy Mechanical Alloying of Immiscible Zr–Cr Alloy, *J. Mater. Res.*, 2020, **35**(14), p 1825–1836.
32. C.F. Sun, Y.C. Guo, Z. Yang, J.P. Li, S.Q. Xi, Z.Q. Jie, and T. Xu, Microstructurally Stable Nanocomposite WTaMoNb/Cu Prepared by Mechanical Alloying and Hot Pressing Sintering, *Mater Lett.* **306**, 4, 130894, (2022) (in English)
33. M. Azimi and G.H. Akbari, Development of Nano-structure Cu–Zr Alloys by the Mechanical Alloying Process, *J. Alloys Compd.*, 2011, **509**(1), p 27–32.
34. V. Nguyen-Hoang and N.T.H. Oanh, Microstructure and Electrical Property of Ex-Situ and In-Situ Copper Titanium Carbide Nanocomposites, *Metals*, 2020, **10**, p 735.
35. J. Zhuang, Y. Liu, Z. Cao, and Y. Li, The Influence of Technological Process on Dry Sliding Wear Behaviour of Titanium Carbide Reinforcement Copper Matrix Composites, *Mater. Trans.*, 2010, **51**, p 2311–2317.
36. J. Zou, D.-P. Lu, Q.-F. Fu, K.-M. Liu, and J. Jiang, Microstructure and Properties of Cu–Fe Deformation Processed in-situ Composite, *Vacuum*, 2019, **167**, p 54–58.
37. G. Shi, X. Chen, H. Jiang, Z. Wang, H. Tang, and Y. Fan, Strengthening Mechanisms of Fe Nanoparticles for Single Crystal Cu–Fe Alloy, *Mater. Sci. Eng., A*, 2015, **636**, p 43–47.
38. H. Gao, J. Wang, D. Shu, and B. Sun, Microstructure and Properties of Cu–11Fe–6Ag in situ Composite after Thermo-mechanical Treatments, *J. Alloy. Compd.*, 2007, **438**(1), p 268–273.
39. P. Qi, X. Liang, Y. Tong, Y. Chen, and Z.J.R.M.M. Zhang, Engineering, Effect of Milling Time on Preparation of NbMoTaW High Entropy Alloy Powder by Mechanical Alloying, *Rare Metal Mater. Eng.*, (2019)
40. P.J.M.S. Xiao, E.o.P. Metallurgy, Influence of Milling Rate and Process control Agents on Mechanically Alloying of Ti-26% Cr, *Rare Metal Mater. Eng.* (2002)
41. F. Wang, Y. Li, K. Wakoh, Y. Koizumi, and A. Chiba, Cu–Ti–C Alloy with High Strength and High Electrical Conductivity Prepared by Two-Step Ball-Milling Processes, *Mater. Des.*, 2014, **61**, p 70–74.
42. Q.-Y. Dong, L.-N. Shen, M.-P. Wang, Y.-L. Jia, Z. Li, F. Cao, and C. Chen, Microstructure and Properties of Cu–23Fe–003P Alloy During Thermomechanical Treatments, *Trans. Nonferrous Metals Soc. China*, 2015, **25**(5), p 1551–1558.
43. Q. Dong, L. Shen, F. Cao, Y. Jia, K. Liao, and M. Wang, Effect of Thermomechanical Processing on the Microstructure and Properties of a Cu-Fe-P Alloy, *J. Mater. Eng. Perform.*, 2015, **24**(4), p 1531–1539.
44. S. Papaefthymiou, M. Bouzouni, and E. Gavalas, Theoretical Study of Particle Dissolution during Homogenization in Cu–Fe–P Alloy, **8**(6), 455 (2018)
45. H. Cao, J.Y. Min, S.D. Wu, A.P. Xian, and J.K. Shang, Pinning of Grain Boundaries by Second Phase Particles in Equal-Channel Angularly Pressed Cu–Fe–P alloy, *Mater. Sci. Eng. A*, 2006, **431**(1), p 86–91.
46. L. Han, J. Liu, H. Tang, X. Ma, and W. Zhao, Preparation and Properties of Ultra-Fine-Grained and Nanostructured Copper Alloy with the Addition of P, *Mater. Chem. Phys.*, 2019, **221**, p 322–331.
47. R.E. Smallman and R.J. Bishop, Preface, Modern Physical Metallurgy and Materials Engineering (Sixth Edition)ed., R.E. Smallman, R.J. Bishop, Eds., Butterworth-Heinemann, 1999, p x
48. Q. Fang, Z. Kang, Y. Gan, and Y. Long, Microstructures and Mechanical Properties of Spark Plasma Sintered Cu–Cr Composites Prepared by Mechanical Milling and Alloying, *Mater. Des.*, 2015, **88**, p 8–15.
49. I. Lahiri and S. Bhargava, Compaction and Sintering Response of Mechanically Alloyed Cu–Cr Powder, *Powder Technol.*, 2009, **189**(3), p 433–438.
50. S. Cui and I.-H. Jung, Thermodynamic Modeling of the Cu-Fe-Cr and Cu-Fe-Mn Systems, *Calphad*, 2017, **56**, p 241–259.
51. Q. Fang and Z. Kang, An Investigation on Morphology and Structure of Cu–Cr Alloy Powders Prepared by Mechanical Milling and Alloying, *Powder Technol.*, 2015, **270**, p 104–111.
52. L. Shan, X. Wang, and Y. Wang, Extension of Solid Solubility and Structural Evolution in Nano-Structured Cu–Cr Solid Solution Induced by High-Energy Milling, **13**(23), 5532 (2020)
53. H. Fernee, J. Nairn, and A. Atrens, Precipitation Hardening of Cu-Fe-Cr Alloys Part I Mechanical and Electrical Properties, *J. Mater. Sci.*, 2001, **36**(11), p 2711–2719.
54. G.H. Akbari and M.T. Dehaqani, Behavior of CU-CR Powder Mixtures during Mechanical Alloying, *Int. J. Eng. Trans. B*, 2010, **23**, p 69–76.
55. F.L. Zhang, C.Y. Wang, and M. Zhu, Nanostructured WC/Co Composite Powder Prepared by High Energy Ball Milling, *Scripta Mater.*, 2003, **49**(11), p 1123–1128.
56. J. Eckert, J.C. Holzer, C.E. Krill, and W.L. Johnson, Structural and Thermodynamic Properties of nanocrystalline fcc metals Prepared by Mechanical Attrition, *J. Mater. Res.*, 1992, **7**(7), p 1751–1761.
57. S. Patra, Gouthama, and K. Mondal, Densification Behavior of Mechanically Milled Cu–8at% Cr Alloy and Its Mechanical and Electrical Properties, *Progress Nat. Sci. Mater. Int.* **24**(6), 608–622 (2014)
58. S. Safi and G.H. Akbari, Evaluation of Synthesizing Nano Particles in Copper Matrix by Mechanical Alloying of Cu-1% Al and Copper Oxide %J, *J. Adv. Mater. Eng.*, 2017, **36**(1), p 71–85.
59. I. Börner and J. Eckert, Structural Properties and Compositional Dependence of Grain Size in Heavily Mechanically Deformed Nanophase NiAl, *Mater. Sci. Forum*, 1996, **225–227**, p 377–382.
60. C. Aguilar, V.D.P. Martinez, J.M. Palacios, S. Ordoñez, and O. Pavez, A thermodynamic approach to energy storage on mechanical alloying of the Cu–Cr system, *Scripta Mater.*, 2007, **57**(3), p 213–216.
61. Y. Jin, K. Adachi, T. Takeuchi, and H.G. Suzuki, Correlation Between the Electrical Conductivity and Aging Treatment for a Cu-15 wt.% Cr Alloy Composite Formed in-situ, *Mater. Lett.*, 1997, **32**(5), p 307–311.
62. L. Lu, M.O. Lai, and S. Zhang, Diffusion in Mechanical Alloying, *J. Mater Process Technol.*, 1997, **67**(1), p 100–104.
63. L. Lu, M.O. Lai, and S. Zhang, Evolution and Characterization of a Ni3Al Intermetallic Compound During Mechanical Alloying, *Mater. Des.*, 1994, **15**(2), p 79–86.
64. G. Veltl, B. Scholz, and H.D. Kunze, Amorphization of Cu–Ta Alloys by Mechanical Alloying, *Mater. Sci. Eng. A*, 1991, **134**, p 1410–1413.
65. A.R. Yavari, P.J. Desrè, and T. Benameur, Mechanically Driven Alloying of Immiscible Elements, *Phys. Rev. Lett.*, 1992, **68**(14), p 2235–2238.
66. M. Vaezi, S. Ghassemi, and A. Shokuhfar, The Effect of Impact Energy on the Formation of Nanocrystalline Powders in Cu50% Fe Immiscible Alloy Systems, *Mater. Sci.—Poland*, **26**, (2008)
67. N. Ravishankar, T.A. Abinandanan, and K. Chattopadhyay, Application of Effective Potential Formalism to Mechanical Alloying in Ag–Cu and Cu–Fe Systems, *Mater. Sci. Eng. A*, 2001, **304–306**, p 413–417.

68. A. Orecchini, F. Sacchetti, C. Petrillo, P. Postorino, A. Congeduti, C. Giorgetti, F. Baudelet, and G. Mazzone, Magnetic States of Iron in Metastable fcc Fe–Cu Alloys, *J. Alloys Compd.*, 2006, **424**(1), p 27–32.
69. L. Han, J. Liu, H. Tang, X. Ma, and W. Zhao, Investigation on the Properties of Nanostructured Cu Alloy Prepared by Mechanical Milling and Reactive Hot-Pressing, *J. Alloys Compd.*, 2018, **742**, p 284–289.
70. F. Wang, Y. Li, X. Wang, Y. Koizumi, Y. Kenta, and A. Chiba, In-situ Fabrication and Characterization of ultrafine structured Cu–TiC Composites with High Strength and High Conductivity by Mechanical Milling, *J. Alloys Compd.*, 2016, **657**, p 122–132.
71. N. Simos, Z. Kotsina, E. Dooryhee, Z. Zhong, H. Zhong, F. Camino, E. Quaranta, N. Charitonidis, A. Bertarelli, S. Redaelli, L. Snead, and D. Sprouster, 200 MeV Proton Irradiation of the Oxide-Dispersion-Strengthened Copper Alloy (GlidCop-A115), *J. Nucl. Mater.*, 2019, **516**, p 360–372.
72. M. Ziemnicka-Sylwester, The Cu Matrix Cermets Remarkably Strengthened by TiB₂ “in situ” Synthesized via Self-Propagating High Temperature Synthesis, *Mater. Des.*, 2014, **53**, p 758–765.

Publisher's Note Springer Nature remains neutral with regard to jurisdictional claims in published maps and institutional affiliations.